CFD INVESTIGATION OF A NOVEL FUEL-SAVING DEVICE FOR ARTICULATED TRACTOR-TRAILER COMBINATIONS

V. Malviya, R. Mishra* and J. Fieldhouse

University of Huddersfield, Queensgate, Huddersfield, HD1 3DH, United Kingdom
* E-Mail: r.mishra@hud.ac.uk (Corresponding Author)

ABSTRACT: Enhancing the aerodynamic efficiency of commercial vehicles is gaining increasing importance as it helps to reduce both overall fuel consumption as well as emissions. This paper investigates the advantages offered by a novel fuel-saving device for such vehicles. This device uses a moving surface to impart additional kinetic energy to flow near the roof surface. The additional momentum in the flow modifies the flow field, thereby significantly reducing pressure drag. Distribution of drag shows that the front and rear faces of the semi-trailer and the tractor cab are the dominant contributors to drag. The overall reduction in drag has been quantified by the distribution of pressure on the surface as well as the individual contribution to drag by each surface of the vehicle. The newly developed device has been shown to be very effective in reducing the fuel consumption of tractor-trailers.

Keywords: momentum injection, computational fluid dynamics, aerodynamic drag, flow-field, fuel-saving, tractor-trailer

1. INTRODUCTION

Fuel consumption has been a critical cause for concern in the entire automotive industry, especially in high-mileage sectors like freight and commercial transport. The global petroleum reserves are reaching saturation and worst-case scenarios predict that a peak or a plateau in global oil output is fast approaching (Roberts, 2008). This plateau in oil production could last for as little as 15 years, after which the global oil production is predicted to fall. The continuously rising demand for oil coupled with decline in its production could mean complete exhaustion of oil reserves before the end of the 21st century.

Continuously rising fuel prices have resulted in increasing pressure on the transport and infrastructure industry to reduce costs. Around 70% of all goods are transported by trucks and a large proportion of these are articulated tractor-trailers. A typical large freight operator in the United Kingdom has approximately 600 tractor units and twice as many semi-trailers. Such a fleet would annually cover about 56 million miles, which translates to approximately £19.25 million in fuel (Department for Transport, 2006). Hence even a 0.25% reduction in fuel consumption translates to about £50000 savings in annual fuel costs.

In most of the cases the drag force (F_D) is the most dominant resistive force and accounts for over 50% of the overall resistance to motion and hence influences the fuel efficiency of the vehicle.

In general vehicle shape influences the aerodynamic force system generated due to the flow field created around it. The resulting velocity and pressure fields around the vehicle affect the magnitudes and directions of various aerodynamic forces and moments such as drag force, lift force, side force, rolling moment, pitching moment and yawing moment. The drag force is the component of the aerodynamic force-moment system which acts opposite to the direction of travel and influences the fuel efficiency of the vehicle. The other components of the aerodynamic force system mainly influence the stability of the vehicle. The drag force increases proportionally with the square of the vehicle speed (V), and the power (P) required to overcome this drag is proportional to the cube of the speed.

Table 1 shows the typical influence of drag on fuel consumption of a typical 40 tonne semi-trailer. It can be seen from this relation that a reduction in drag has a potential to contribute to significant savings in fuel.

Over 90% of the drag force acting on the vehicle is contributed by the non-uniform pressure field (also called form drag). The remainder of the drag force is caused by skin friction due to shear stress at surfaces (also called viscous or friction drag). The aerodynamic drag on vehicles can be reduced by making the body streamlined and thus reducing the form drag. The form drag can also be reduced by controlling the separation of flow where shape alteration is not possible. Flow

Table 1 Influence of drag on fuel consumption of a 40-tonne semi-trailer (Hucho, 1998).

C_D Reduction	Fuel Saving			
	Level Road	Hilly motorway	Highway	Very difficult route
0	0	0	0	0
5	1.75	0.50	0.33	0.17
10	3.50	1.00	0.66	0.33
15	5.25	1.50	1.00	0.50
20	7.00	2.00	1.33	0.66
25	8.75	2.50	1.67	0.83
30	10.50	3.00	2.00	1.00
35	12.25	3.50	2.34	1.17

separation in the boundary occurs when the kinetic energy of the flow in the boundary layer is not sufficient to overcome the adverse pressure gradient. Tractor-trailer combinations increase the complications for flow-field analysis as they consist of two discrete bluff bodies in tandem. Manipulating the vehicle shape is severely restricted for commercial vehicles by mainly legal and practical guidelines, such as limitations on maximum length and maintaining a minimum gap between the tractor unit and the semi-trailer (RoadTransport.com, 2007). Analysis is made further complicated by the current trend of semi-trailers moving toward the double-deck layout to enhance the payload/fuel ratio (Department for Transport, 2006). This provides an opportunity to use add-on devices to reduce aerodynamic drag thereby reducing the fuel consumption.

Several techniques have been applied over the last few decades to delay the separation of the boundary layer and hence reduce drag; the simplest of them is the rounding of the leading edges of the vehicle (Allan, 1981). Further efforts in altering the shape of semi-trailer units lead to significant reduction in drag (DON-BUR n.d.), but they also accompany with significant penalty on payload capacity and interfere with loading operations as compared to standard double-deck semi-trailers. Hence one of the most popular techniques is to use add-on devices to manage the drag force and hence the fuel consumption while maintaining/increasing the payload capacity (Rose, 1981; Matěj & Jiří, 2004; Englar, 2000). The performance of a number of add-on devices like cab roof fairing, front air dams and air-turning vanes was comparatively quantified by Rose (1981) by performing full-scale experiments on a modified rigid commercial truck. The efficiency of the tested add-on devices was quantified both in terms of reduction in drag coefficient as well as reduction in overall fuel consumption. It was reported that more than 18% of the fuel savings due to these add-on devices were achieved on motorways whereas an average saving of over 13% was achieved for mixed driving conditions. It was also shown that increased downward flow in the tractor-trailer gap reduces overall drag as it results in higher under-body velocities causing higher pressure downstream of the vehicle. These results were obtained from full-scale wind tunnel tests and hence severe limitations were noticed in terms of blockage, closeness of boundaries and replicating actual flow conditions. In particular excessive blockage of up to 10% and the consequent interference of the test section roof with the flow field of the vehicle were seen to affect the results.

Allan (1981) demonstrated the importance of pressure distribution in the flow field around a scaled model of a tractor-trailer combination and showed the influence of ground proximity and gap width between the tractor cab and the trailer on the overall aerodynamic drag. Allan (1981) also investigated the effect of rounding of edges of the tractor cab on the overall drag. Two air deflecting devices were also investigated with varying degree of success. In this work the relevance of the results to real-world situations was observed to be fairly limited. This is because of the use of a significantly simplified model which consisted only of two discrete boxes separated by an open space (bridging section was absent) which allowed the flow from the tractor-trailer gap to pass rearward underneath the trailer. The model did not incorporate wheels thus affecting the accuracy of the results because wheels would affect the flow field of the model especially under the body (Régert & Lajos, 2007). Moreover, practical limitations prohibited measurement of individual pressure distribution on all the faces of the model thereby limiting the analysis. The overall drag was computed by

integrating the surface pressure distribution and the friction drag was not considered in this analysis.

Matěj and Jiří (2004) performed an aerodynamic optimisation study of a scaled 1:15 model of a semi-trailer unit by investigating several under-body drag-reducing add-on devices like side-skirts, wheel covers and under-body covers. A fairly limited computational fluid dynamic (CFD) investigation of a rear-end tapering device was also performed.

Most of the above mentioned add-on devices had several inherent limitations. Some of these devices were primitive in nature and the design of others did not allow their use with varying dimensions of trailer units. Moreover, some shape altering add-on devices like tapered boat tails (Matěj & Jiří, 2004) encounter problems during loading and manoeuvring due to the excess length and hence are not suitable for practical applications. In the literature several papers have been found that report work on a novel aerodynamic technique, momentum injection or moving surface boundary layer control (MSBC) to improve aerodynamic efficiency of the commercial vehicles (Allan, 1981; Rose, 1981; Malviya, Mishra & Fieldhouse, 2008). Modi (1991), Modi, Fernando & Yokomizo (1991) and Modi, Ying & Yokomizo (1992) investigated the parametric influence of injection of momentum into the flow on the drag reduction on bluff geometries, particularly flat plate, D-section and prisms. An optimisation study of the application of momentum injection on articulated commercial vehicles was also carried out (Modi, 1997). Various combinations of moving surfaces were reported to achieve reduction drag of up to 24%.

Munshi, Modi & Yokomizo (1999) analysed the pressure distribution, resultant forces, flow structures and wake characteristics of the effect of momentum injection on flat plates and rectangular prisms. It was reported that the resultant decrease in drag due to momentum injection was associated with an increase in wake pressure. These investigations suggest that the power consumed by a moving surface installed on a typical large tractor-trailer would be about 1.8 kW, which is less than 0.5% of the engine power. This is significantly lower than the power required to drive other active techniques of boundary layer control like suction.

Singh et al. (2005) have also investigated the application of momentum injection to tractor-trailers by performing wind tunnel experiments and two-dimensional CFD studies of two discrete boxes representing a tractor and a trailer in tandem. They analysed the influence of MSBC on overall drag by examining two rotating cylinders of different diameters at two different speeds of rotation. The optimisation of momentum injection applied to the two-dimensional tractor-trailer combination achieved a reduction in drag of up to 35%. However, the results were obtained by ignoring the under-body flow and the model was placed on the ground. Moreover, the investigation did not account for semi-trailer units that are higher than the tractor cab (e.g., double-deck semi-trailers).

Several of the above studies were limited by the highly simplified models used (Allan, 1981; Rose, 1981; Modi, 1997; Singh et al., 2005), which raised doubts regarding the relevance of the results to real conditions. Others were limited by the scope of experimental testing and related errors like test section blockage (Rose, 1981) and insufficient measured data (Allan, 1981). As previously mentioned MSBC can be used to actively control the flow of air past a semi-trailer with or without other add-on devices such as cab roof fairing. In the present investigation a momentum injection device has been developed that improves the aerodynamic efficiency of the vehicle by modifying the flow field and the separation behaviour of the boundary layer. This device has been developed with an aim of providing reduction in aerodynamic drag with least impact on operational or payload capacity. The device incorporates a rotating cylinder mechanism at the top leading edge of the semi-trailer. It is simple in assembly and can be retrofitted to existing vehicles as well.

The present investigation employs three-dimensional CFD techniques using commercially available CFD code *Fluent®* (Fluent Inc., 2006) to overcome the practical limitations imposed by experimental testing and uncertainties related to models that may not represent real conditions. The CFD code has been validated using flow field measurements in a wind tunnel.

2. METHODOLOGY

Figure 1 shows the proposed MSBC device that incorporates a rotating cylinder into the top leading edge of the semi-trailer. Integrated motor assemblies are then used to drive the cylinder. This system modifies the flow field by providing additional kinetic energy to the air flow near the surface and hence inhibits the tendency of flow to separate at the top of the semi-trailer because of the presence of adverse pressure gradient. At the same time it relieves pressure from the front face

of the semi-trailer in the gap facing the flow. The device modifies the flow pattern in the gap between the tractor and trailer considerably and hence reduces the overall drag considerably (Allan, 1981).
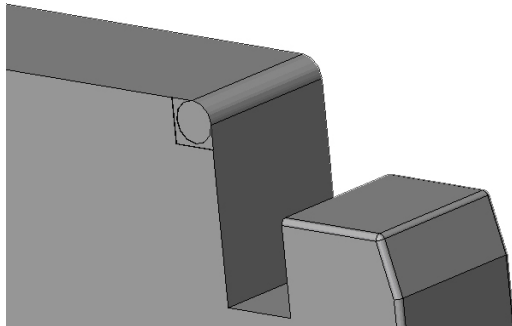

Fig. 1   Schematic representation of proposed MSBC system installed on a double-deck semi-trailer unit.

To quantify the effectiveness of the developed system over and above existing systems the following four configurations of a tractor-trailer combination have been investigated in the present analysis:

• Semi-trailer with no devices – baseline configuration for reference (Fig. 2(a)).

• Semi-trailer with cab roof fairing (Fig. 2(b)).

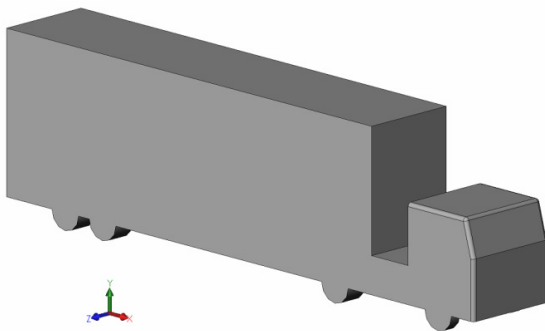• Semi-trailer with the proposed MSBC system (circled, Fig. 2(c)).

• Semi-trailer with the cab roof fairing and proposed MSBC system (Fig. 2(d)).

Typical cruising speeds of heavy commercial vehicles (HCV) range from 40 mph to 50 mph (18 m/s to 22 m/s). The velocity of tractor-trailer combination in this study has been taken to be 19.5 m/s (70 km/hour, 43 mph) as per the reference (Department for Transport, 2006). Reynolds number (Re) based on the width (Singh et al., 2005) ($w = 2.6$ m) of the vehicle is 3.45×10^6. The angle of attack of the flow has been maintained at 0° for all four configurations tested.

Figure 3 shows details of the simplified model of the baseline condition of a generic tractor-trailer combination developed in a computer-aided design (CAD) software package. This baseline condition represents the reference geometric configuration of the combination without any aerodynamic drag-reducing devices. The model was chosen such that the tractor cab and the trailer are not discrete bluff bodies but are joined by a bridging section between the tractor and the trailer. This bridging section prevents flow in the gap from escaping under the trailer and thus prevents any inaccuracies as seen in earlier studies (Allan, 1981; Modi, 1997). The standard dimensions (see Fig. 3) of the tractor cab, semi-trailer, wheels, ground clearance as well as the

Fig. 2(a)   Baseline configuration of the tractor-trailer combination.
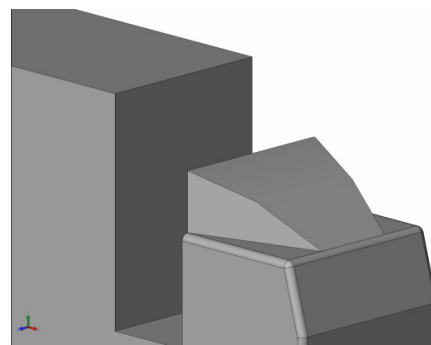

Fig. 2(b)   Configuration of the tractor-trailer combination with the cab fairing only.
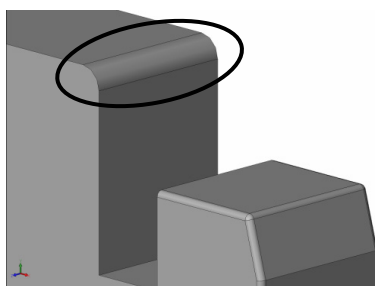

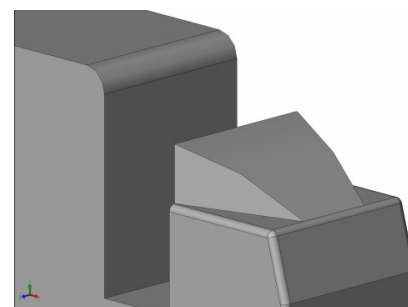Fig. 2(c)   Configuration of the tractor-trailer combination with the MSBC system only.

Fig. 2(d)   Configuration of the tractor-trailer combination with the cab fairing and the MSBC system.

tractor-trailer gap are typical of real conditions. The edges of the cab have been rounded with a radius of 0.1 m.
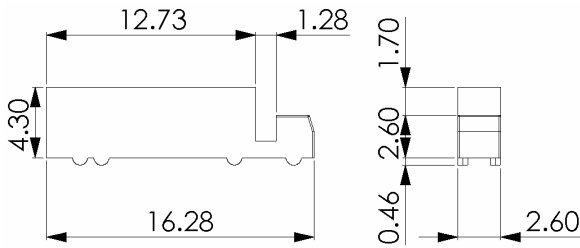

Fig. 3   Dimensions of baseline tractor-trailer model (m).

The diameter of the rotating cylinder considered in this study has been taken as 0.7 m. This was consistent with the "cylinder diameter/trailer length" ratio used by Singh et al. (2005). For a reasonable basis for comparison with other drag-reducing devices, the vehicle (hence free stream) velocity (V_{air}) in this study was taken as 19.5 m/s (43.5 mile/hour, 70 km/hour). The linear velocity ($V_{cylinder}$) at the surface of the rotating cylinder was taken as 3.9 m/s which is equal to the $V_{cylinder}/V_{air}$ ratio (λ=0.2) considered by Singh et al. (2005). Hence the angular velocity of the cylinder ($\Omega_{cylinder}$) is 11.14 rad/s ($\approx$106 rev/min).

3.   NUMERICAL FORMULATION

The flow field of the tractor-trailer model is simulated using CFD. This includes solving a set of partial differential equations with predefined boundary conditions. The CFD package *Fluent® 6.3* (Fluent Inc., 2006) is used to iteratively solve time averaged momentum equations along with the continuity equation and appropriate auxiliary equations depending on the type of applications using a control volume formulation. In this study the equations for conservation of mass and momentum have been solved sequentially with two additional transport equations for steady turbulent flow. Linearisation of the governing equations is implicit. The *SIMPLE* pressure-based segregated algorithm was used for pressure-velocity coupling to prevent instability of the solution due to relatively high skewness of mesh elements that was expected around the tyre patch of the wheels. Pressure interpolation was done using the *Standard* scheme. Discretisation of the momentum equations was done by using the *Second Order Upwind* scheme to achieve higher accuracy of flow variables at each cell face.

3.1   Mass conservation

The mass conservation equation given below is valid for both incompressible and compressible flows (Fluent Inc., 2006). The source term S_m is the mass added to the continuous phase from the dispersed second phase (e.g., due to vaporisation of liquid droplets) and any user defined sources

$$\frac{\partial \rho}{\partial t} + \nabla \cdot (\rho \vec{v}) = S_m \qquad (1)$$

3.2   Momentum conservation

Conservation of momentum in the ith direction in an inertial (non accelerating) reference frame is given by

$$\frac{\partial (\rho \vec{u})}{\partial t} + \nabla (\rho \cdot \vec{v} \cdot \vec{v}) = -\nabla p + \nabla (\bar{\bar{\tau}}) + \rho \vec{g} + \vec{F} \qquad (2)$$

The stress tensor is given by

$$\tau_{ij} = \mu \left[(\nabla \vec{v} + \nabla \vec{v}^{T}) - \frac{2}{3} \nabla \vec{v} I \right] \qquad (3)$$

where μ is the molecular viscosity, I is the unit tensor, and the second term on the right hand side is the effect of volume dilation (Fluent Inc., 2006). *Fluent®* uses the *finite volume method* to solve the time-averaged *Navier-Stokes* equations and is known for its robustness in simulating many fluid dynamic phenomena. The *finite volume method* consists of three stages; the formal integration of the governing equations of the fluid flow over all the (finite) control volumes of the solution domain. Then discretisation, involving the substitution of a variety of finite-difference-type approximations for the terms in the integrated equation representing flow processes such as convection, diffusion and sources. This converts the integral equation into a system of algebraic equations, which can then be solved using iterative methods (Fluent Inc., 2006). The first stage of the process, the control volume integration, is the step that distinguishes the *finite volume method* from other CFD methods. The statements resulting from this step express the conservation of the relevant properties for each finite cell volume (Versteeg & Malalasekera, 1995).

3.3   Computational domain

The various models of the tractor-trailer combinations to be investigated were each imported into a three-dimensional flow domain created in *Gambit®* (Fluent Inc., 2007). The flow domain consists of a rectangular cuboid volume

which contains the tractor-trailer model as shown in Fig. 4. The length of the flow domain was *179* m, such that the inlet of the flow domain was 3·*l* upstream of the tractor-trailer model (where *l* is the overall length of the tractor-trailer model). The outlet of the domain was 7·*l* downstream of the tractor-trailer model. It was found that 7·*l* downstream of the model was spatially sufficient to prevent the downstream-imposed constant pressure of 101325 Pa (ambient atmospheric pressure) from having an upstream effect on the pressure field (Régert & Lajos, 2007). The width of the flow domain was *18.2* m, such that the longitudinal side walls of this domain were at a distance of *3 w* from the model (where *w* is the overall width of the tractor-trailer model). This was found sufficient to prevent the interference of the domain wall boundary layer with the flow-field of the model. Similarly, the height of the flow domain was *22* m such that the distance between the horizontal top wall of the domain and the top surface of the semi-trailer was at least 4·*h* (where *h* is the overall height of the tractor-trailer combination). The cross-sectional blockage ratio was found to be 3.1% based on a flow domain cross section area of 400.4 m^2 and model cross section area of 12.22 m^2. Since the blockage was less than 5% no corrections were required (Singh et al., 2005).
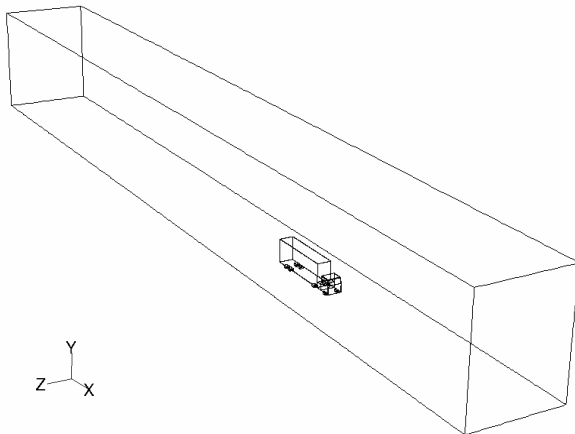

Fig. 4   Computational domain.

3.4   CFD mesh scheme

This resultant flow domain was discretised in *Gambit®* (Fluent Inc., 2007) into an unstructured mesh of hybrid tetrahedral cell elements with an element count of approximately 2.2 million elements. Mesh quality was controlled such that the vehicle model surface and consequently its expected flow-field consisted of smaller elements to increase resolution and ensure reliable results.

The resultant mesh achieved a maximum skewness of 0.6 for over 95% of the elements and an aspect ratio between 1 and 2 for over 99% of the elements.

3.5   CFD parameters

An initial comparison of the two most popular two-equation turbulence models, the *realizable k-ε* (Shih et al., 1995) and the *SST k-ω* (Menter, 1994) models, was carried out to choose the model with higher accuracy for this analysis. Both these models are claimed to predict with reasonable accuracy the characteristics of separated flow (Régert & Lajos, 2007). With coefficient of drag (C_D) as the reference parameter, it was found that the *SST k-ω* model provided reasonably accurate results. On the other hand, *realizable k-ε* failed to converge to stable residual values for the given meshing scheme. This comparison could have been further studied by increasing the mesh resolution of the flow domain; however the additional accuracy gain was not sufficient to justify the additional penalty on computational time imposed by the large mesh. Hence *SST k-ω* was chosen for the analysis. Convergence criteria for the residuals of the transport equations were set to 1×10^{-4}; these criteria was deliberately set too low to ensure that the accuracy was being limited by the chosen mesh scheme only. Wall roughness for all wall boundaries in the flow domain was ignored and all the wall faces were taken to be smooth.

3.6   Boundaries

The lateral face of the domain ahead of the tractor-trailer model was defined as a velocity inlet at a constant velocity of 19.5 m/s (70.2 km/hour, 43.6 mph). The lateral face of the domain behind the model was defined as a pressure outlet at constant atmospheric pressure of 101325 Pa. The bottom face of the flow domain was defined as a moving wall, synchronised with the inlet flow velocity at 19.5 m/s in the streamwise direction to avoid formation of its own boundary layer which could otherwise modify the flow under the vehicle model. The wheels of the model were defined as moving walls with an angular velocity of 48.75 rad/s about the respective axles/axes to synchronise them with the relative motion of the vehicle. In case of the tractor-trailer with the MSBC system, the curved face of the rotating cylinder was defined as moving wall with an angular velocity of 11.14 rad/s about the axis of the cylinder.

4. VALIDATION OF CFD

The drag coefficient of the baseline configuration of the tractor-trailer combination was found to be 0.9 which is consistent with literature. To further establish the level of accuracy of the CFD results, flow field around a scaled model of the baseline configuration of the tractor-trailer model was experimentally measured in a wind tunnel. Coefficient of pressure (C_p) was taken as a reference parameter on a vertical rake located $0.2 \cdot l$ upstream of the model. Comparison of this pressure profile along the height of the rake was carried between the wind tunnel and CFD simulations. The scope of experimental measurements possible is generally limited in representing real conditions. The wind tunnel experiments were hence restricted only to validate the CFD code.

4.1 Experimental setup

The validation benchmark experiment was carried out in the low speed wind tunnel at the University of Huddersfield. The wind tunnel is of open circuit type and has a 1.5 m long test section with a 0.6 m × 0.6 m cross section. Air is provided by an axial blower fan with pneumatically adjustable variable blade pitch. The range of air speeds possible in the wind tunnel was from 7 m/s to 19.2 m/s. The bottom of the test section was provided with mounting holes and openings for inserting flow measuring devices.
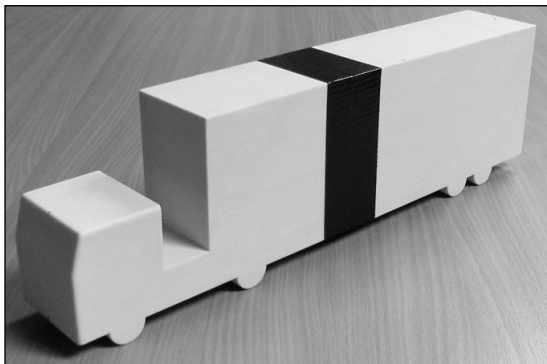

Fig. 5   1:40 scale model of baseline tractor-trailer combination.

The model investigated was a 1:40 scale model of the baseline tractor-trailer configuration made from compacted powder using a 3D printer (see Fig. 5). The dimensions of the model were 0.407 m × 0.065 m × 0.119 m (length × width × height). The wheels of the model were stationary and the model was mounted on

the bottom of the test section. Flow measurement was done by a four-hole cobra probe of a tip diameter of 1.5 mm, connected to a computer workstation with associated data acquisition software. The benchmark tests were conducted at a wind tunnel speed of 19.2 m/s. The corresponding Reynolds number relative to the width of the model is 8.7×10^4. This, along with the full-scale Reynolds number of 3.45×10^6 (discussed earlier) are both in the turbulent regime, hence no Reynolds number corrections were applied. The measured turbulent intensity was 3%. The cross-sectional blockage ratio was found to be 2.25% based on a flow domain cross section area of 0.36 m^2 and model cross section area of 8.1×10^{-3} m^2. Since the blockage was less than 5% no corrections were required (Singh et al., 2005).

4.2 Benchmark CFD setup

For validation purposes the flow field around baseline configuration of the tractor-trailer combination (Fig. 2(a)) was simulated with stationary wheels and no moving ground simulation. This was done to accurately reproduce wind tunnel test conditions. The domain inlet boundary was defined for a free stream air velocity of 19.2 m/s with a turbulence intensity of 3% (measured from wind tunnel experiment) and the domain outlet was defined at ambient pressure of 101325 Pa.

4.3 Validation results

Figure 6 shows a comparison of pressure profile upstream of the model. The point of measurement was located 0.08 m upstream of the front face of the tractor cab of the model. This corresponds to a full scale distance of 3.24 m. The vertical height y above the ground has been converted to non-dimensional form relative to the height of the semi-trailer $h_{trailer}$, and measured from the bottom of the vehicle. Negative values of the abscissa indicate the height of the point of interrogation being lower than the bottom of the vehicle. The pressure has been presented on the vertical axis in terms of the non-dimensional coefficient of pressure (C_p).
It can be seen from the profile of the C_p that there is a good correlation between the experimental and CFD results. Higher values of C_p are observed near the ground and up to a height of $0.31 \cdot h_{trailer}$ due to the front face of the cab experiencing higher pressure. Values of pressure above this height decrease almost linearly with increase in height. A maximum deviation of 1.9%

is seen at a height of $0.45 \cdot h_{trailer}$, which can be attributed to experimental errors in positioning the cobra probe at the correct attitude relative to the free stream. It can, however, be concluded at this stage that the computational domain, the mesh scheme, CFD parameters and the boundary conditions are reliable to provide sufficient accuracy for the purpose of the present work.
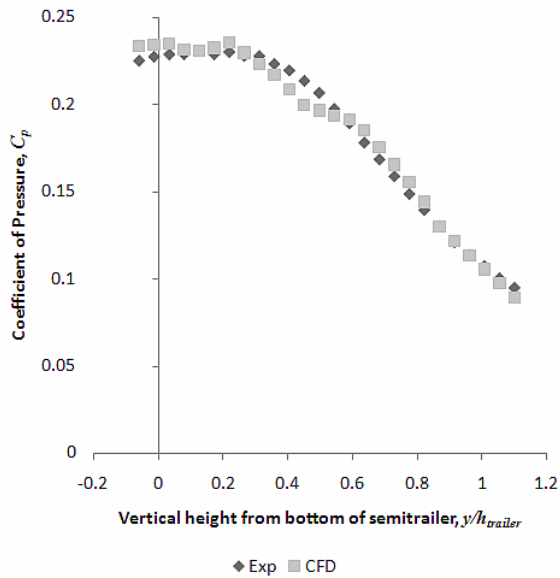

Fig. 6 Comparison of pressure along vertical rake upstream of model.

5. RESULTS AND DISCUSSION

The CFD analysis of flow around the baseline configuration showed that the drag coefficient of the baseline configuration without any add-on devices was found to be 0.9 which agrees well with previous research (Wood & Bauer, 2003) for standard tractor-trailer combinations. This matches well with earlier validation exercise and gives confidence in the correctness of our model.

Apart from the overall coefficient of drag of the tractor-trailer combination, which was based on its frontal area of 12.22 m², the drag contribution of the tractor, trailer and individual faces on the front, top, back and sides of both the tractor and trailer were also computed to quantify the effect of each of the two drag-reducing devices compared as well as that of their combination. The individual drag coefficients of the semi-trailer unit and the tractor cab were found to be 0.57 and 0.26 respectively. Similarly the drag coefficient of the wheels was found to be 0.07. The individual values of drag coefficients indicate that over 63% of the overall drag is contributed by the semi-trailer and almost 29% by the tractor cab. The contribution of the wheels to the overall drag was found to be relatively low at 7%.

Figure 7 shows path lines near the leading edge of the semi-trailer showing separation of flow. This indicates that the flow past the tractor cab is fairly complex.
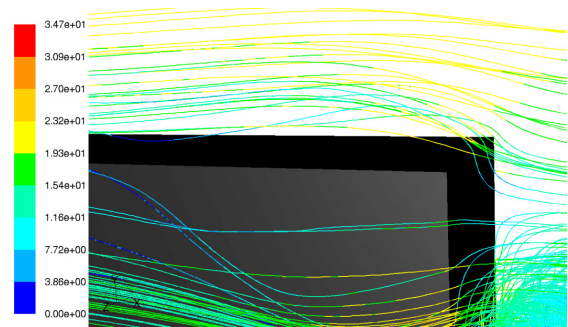

Fig. 7 Flow divergence at semi-trailer edge shown by path lines coloured by velocity magnitude.

Table 2 Individual drag contribution by each surface of the semi-trailer and tractor cab.

Unit	Surface	Drag Coefficient	Contribution to Overall Drag
Semi-trailer	Front	0.3590	39.88%
	Top	0.0024	00.27%
	Rear	0.1896	21.07%
	Bottom	0.0035	00.39%
	Left	0.0077	00.85%
	Right	0.0074	00.82%
Tractor cab	Front	0.2760	30.67%
	Rear	0.0159	01.77%
	Top	-0.0330	-03.67%
	Bottom	0.0003	00.03%
	Left	0.0001	00.01%
	Right	0.0003	00.03%

A further break-up of the drag contribution by each face of the semi-trailer and the tractor cab is shown in Table 2. It can be seen from this itemisation that the main contributors to overall drag of the semi-trailer unit are the front and rear faces of the semi-trailer. To investigate this further the flow around the semi-trailer has been analysed in detail. Just like the semi-trailer, the front and the rear faces of the tractor cab too are the primary contributors to drag. Moreover, it can observed that the top surface of the tractor cab (the roof) exhibits a negative drag of particularly high value, forming over *3*% of the overall drag but in the direction of travel. Initial flow visualisations showed formation of a recirculation bubble, also noted by Allan (1981), due to early separation at the leading edges of the tractor cab. These flow structures will be discussed later.

A large contribution to overall drag by the rear face of the tractor cab and the front face of the semi-trailer has been observed from Table 2. These surfaces respectively form the upstream and the downstream extremities of the tractor-trailer gap.

5.1 Distribution of pressure

Detailed investigation of pressure distribution on these critical surfaces of the vehicle is essential to quantify the effects of flow structures and their effects on the overall pressure drag. Pressure values measured across the flow domain were represented in non-dimensional form by using the expression for coefficient of pressure (C_p) as:

$$C_p = \frac{p - p_\infty}{q_\infty} \tag{4}$$

where

p ≡ local static pressure

p_∞ ≡ free-stream static pressure

q_∞ ≡ free-stream dynamic pressure

$$q_\infty = \frac{1}{2} \cdot \rho \cdot U_\infty^2 \tag{5}$$

Pressure distribution on the front and rear surfaces of the semi-trailer was mapped and plotted on isobar charts as shown in Fig. 8(a) and (b) respectively. The front face (Fig. 8(a)) exhibits fairly symmetric distribution of the pressure about the central X-Y symmetry plane. It can be observed that the symmetry may be due to the 0° relative angle of attack of the air stream. The lower region of the face shows a small region of high pressure (C_p values more than 0.743) covering about 40% of the width. As height along this face increases the C_p reduces to a value of less than -0.0267. Along the top of the front face of the semi-trailer a region of very high pressure can be seen and this region has C_p values in excess of 0.743. This region lies at a height of approximately $0.8 \cdot h_{gap}$ from the bottom of the tractor-trailer gap (where h_{gap} is the vertical height of the gap, from the bottom of the semi-trailer front face to its top leading edge). The rear face of the semi-trailer (Fig. 8(b)) also shows a strong symmetry about the longitudinal X-Y symmetry plane of the vehicle except near the top 20% of the face. Near the bottom of the face values of C_p less than -0.4 are observed. C_p rises to -0.15 near the top 20% of the rear face of the semi-trailer.
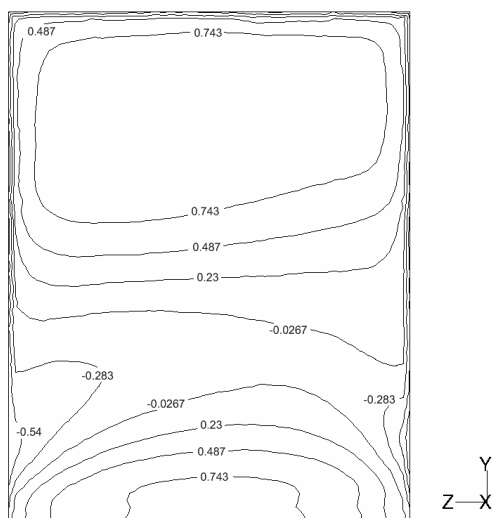

Fig. 8(a)   Pressure distribution on the front face of semi-trailer.
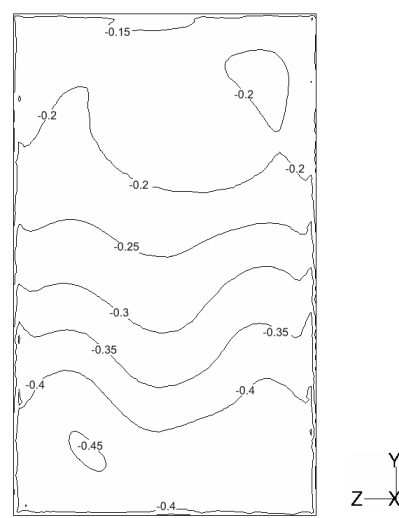

Fig. 8(b)   Pressure distribution on the rear face of semi-trailer.
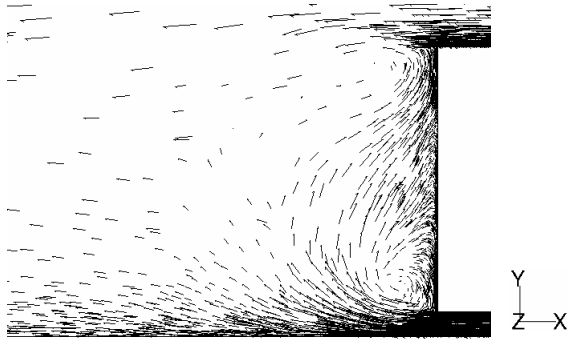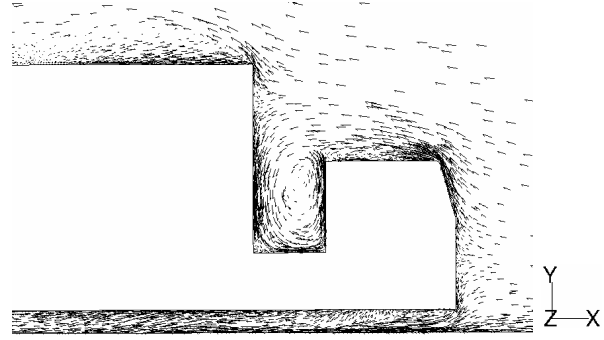
Fig. 9(a)   Semi-trailer wake flow pattern.

Fig. 9(b)   Tractor-trailer gap flow pattern.

The distribution of pressure on both front and rear faces of the semi-trailer is non-linear and predominantly symmetrical about the longitudinal symmetry plane. Overall pressure distributions on both the front and rear faces of the semi-trailer indicate a significant difference. This difference in pressures on the front and rear faces of the vehicles is the primary cause for the pressure drag discussed earlier.

Figure 9(a) shows flow vectors in the wake of the vehicle. The flow pattern shows a pair of contra rotating vortices formed by the square back of the semi-trailer. The lower clockwise vortex is seen to be larger than the upper counter-clockwise vortex. This behaviour is normally seen in square back vehicles (Hucho, 1998). Velocity vectors depicting flow structures around the tractor cab and in the tractor-trailer gap are shown in Fig. 9(b). These vectors show the effect of air stream impacting the upper region of the front face of the semi-trailer and hence creating a high pressure region as discussed earlier (Fig. 8(a)). This figure also shows early separation of the flow at the leading edge of the tractor cab. This leads to formation of the recirculation bubble which causes favourable friction drag on the roof of the cab which is also observed in the negative drag values for the top surface of the tractor cab (also seen in Table 2 earlier). The recirculation bubble trapped in the tractor-trailer gap is also clearly evident from Fig. 9(b).

Figure 9(b) also shows the separated flow at the leading edge of the semi-trailer resulting in a larger recirculation on the top of the semi-trailer roof. This flow near the top surface of the semi-trailer was found to reattach further downstream. The separation and reattachment of the boundary layer flow on the roof of the semi-trailer is described in the following section.
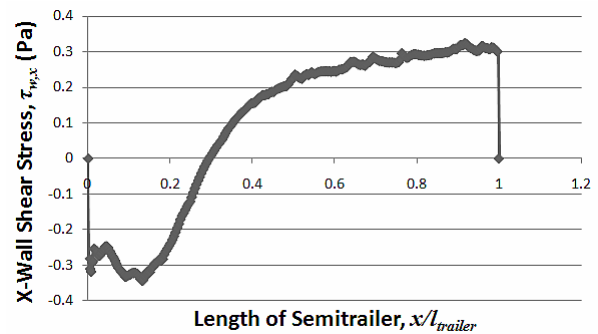

Fig. 10   Streamwise wall shear stress profile on the top surface of the semi-trailer.

5.2   Flow separation

Knowledge of point of flow separation and possible re-attachment along the roof of the semi-trailer is essential for analysing and comparing the flow structures present near the top surface. The flow separation has been shown to affect the wake flow pattern as well (Munshi, Modi and Yokomizo, 1999) which affects the overall pressure drag. The location at which flow separates is the location along the surface in the streamwise direction at which the velocity gradient of the flow on the surface reduces to zero and subsequently velocity changes the direction. Shear stress at the surface (wall shear) and its direction is representative of the velocity in the near vicinity of the surface. Fig 10 shows a distribution of streamwise wall shear stress $\tau_{w,x}$, at various points in the streamwise direction x. This wall shear is measured from the leading edge of the semi-trailer and non-dimensionalised by its length $l_{trailer}$. Shear stress at both the leading and the trailing edges is zero. It is seen that shear stress at the wall acts in a direction opposite to the direction of the free stream up to $x/l_{trailer} = 0.295$. This shows that flow separates at the leading edge of the semi-trailer. As the distance along the roof of the semi-trailer increases the shear stress on the wall increases up to a point where it changes

direction. A closer look at the region of $x/l_{trailer}$ between 0.27 and 0.31 shows that the $\tau_{w,x}$ changes direction at $x/l_{trailer} = 0.295$, indicating that reattachment takes place at $x/l_{trailer} = 0.295$.
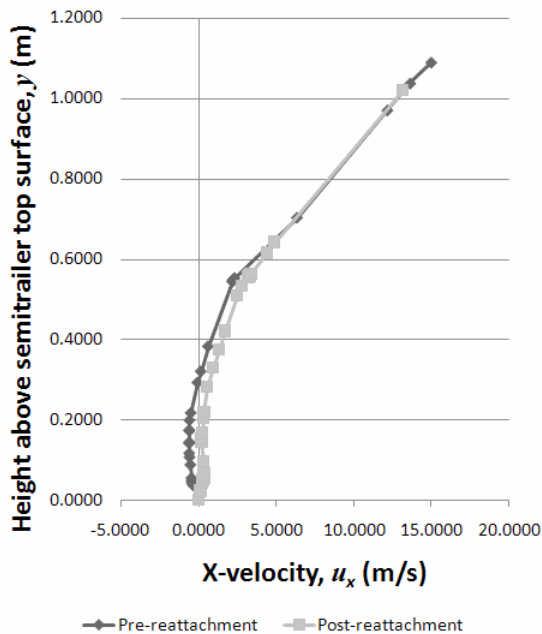

Fig. 11   Streamwise (x) velocity profile in boundary layer of semi-trailer roof.

The correctness of location of re-attachment point has been further validated by Fig. 11 which shows the boundary layer velocity profile plotted before and after the reattachment point at $x/l_{trailer}$ values of 0.29 and 0.30 respectively. The streamwise velocity profile before reattachment shows negative velocity up to a height of 0.27 m from the top surface of the semi-trailer and that after reattachment shows consistently positive streamwise velocities in the entire boundary layer. The above discussion has clearly indicated various features of the flow field around the baseline configuration of tractor-trailer. In the following discussion effect of the developed device on flow features as well as drag contribution of various parts of the tractor-trailer combination has been enumerated.

5.3   Effect of drag-reducing devices

The use of drag-reducing devices can be expected to show a significant change in the flow-field around the tractor-trailer combination discussed earlier. These forced changes through the use of add-on devices in the pressure and velocity fields in the vicinity of the vehicle are intended to reduce the overall drag.

Figures 12 to 14 show isobar plots for the front and rear faces of the semi-trailer with various combinations of drag-reducing add-on devices described earlier. Figures 12(a) and (b) respectively show the pressure distribution on the front and rear faces of the semi-trailer with the cab fairing only. Just like the front face of the baseline semi-trailer shown in Fig. 8(a), Fig. 12(a) also shows symmetric distribution of pressure on the front face of the semi-trailer about the vertical centre line. The lower region of this face exhibits a similar area of high pressure of $C_p = 0.743$, as the baseline configuration (Fig. 8(a)). The pressure on the face shows a much lower value of C_p between -0.283 and -0.54 near the centre of the semi-trailer front face, as compared to the baseline configuration (Fig. 8(a)). Two regions of pressure lower than $C_p = -0.54$ are also seen an either side of the face near the bottom. This is significantly lower than values of C_p for the baseline configuration observed to be between -0.0267 and -0.283. The most prominent difference due to the addition of the cab fairing is a significant reduction in the height of the high pressure region near the top of this face which now, extends from a height of $0.7 \cdot h_{gap}$ to $0.9 \cdot h_{gap}$. This is primarily due to the cab roof fairing shielding a larger area of the front face of the semi-trailer from the oncoming air stream. Moreover, the cab fairing deflects the flow higher up on to the front face of the semi-trailer resulting in upward shift of higher pressure region.
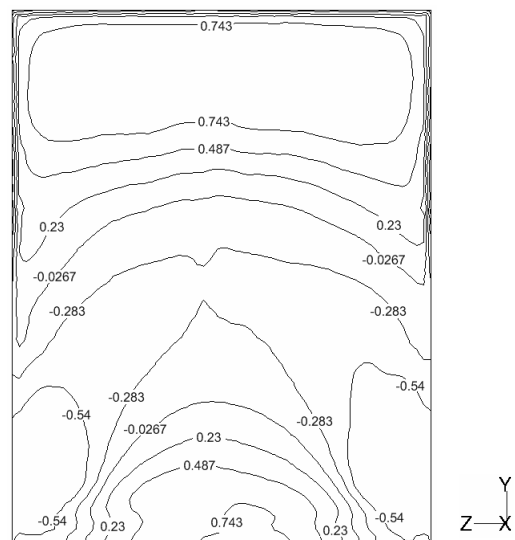

Fig. 12(a)   Pressure distribution on the front face of semi-trailer with cab fairing only.

Figure 12(b) shows the pressure distribution on the rear face of the semi-trailer for the configuration with the cab roof fairing. A low pressure region with C_p less than -0.45 is

observed to extend from a height of $0.04 \cdot h_{trailer}$ to $0.15 \cdot h_{trailer}$. This is 10% lower as compared to the baseline configuration (Fig. 8(b)). Further it is seen that qualitatively the pressure distribution is substantially similar to the baseline configuration for the middle region that extends from a height of $0.25 \cdot h_{trailer}$ to $0.65 \cdot h_{trailer}$. The upper 30% ($0.65 \cdot h_{trailer} < y < 0.95 \cdot h_{trailer}$) of the semi-trailer rear face shows a region of low pressure with C_p values in the range of -0.2 and -0.25 towards the left side of the face.
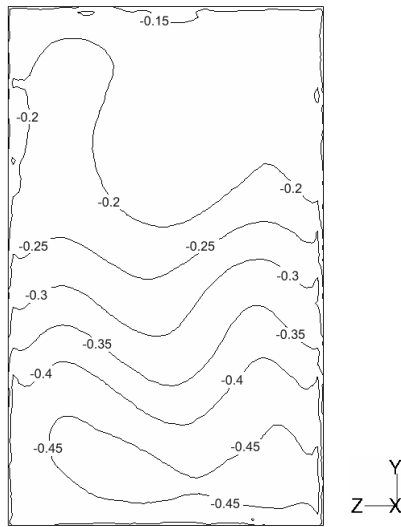

Fig. 12(b) Pressure distribution on the rear face of semi-trailer with cab fairing only.

Figure 13(a) shows the pressure distribution on the front face of the semi-trailer with the MSBC system only. Distribution of pressur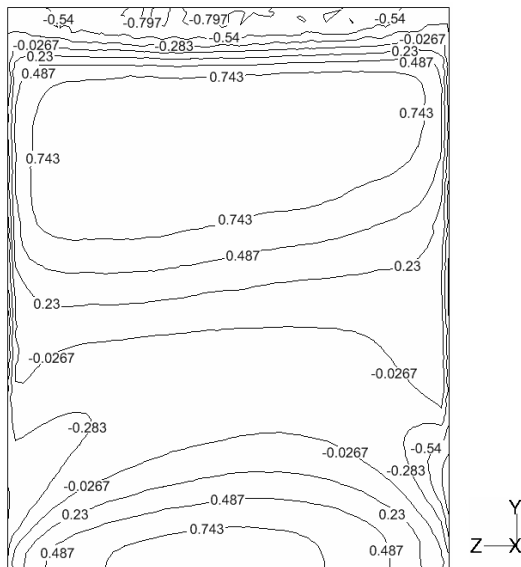e in the lower region of the front face shows substantial similarity with that for the baseline configuration (Fig. 8(a)) where values of C_p at the bottom are in excess of 0.743 and falls to values between -0.0267 and -0.283 in the lower middle region that extends from a height of $0.2 \cdot h_{gap}$ to $0.4 \cdot h_{gap}$. Pressure starts to rise up to a height of $0.7 \cdot h_{gap}$ after which C_p is observed to be in excess of 0.743. At a height of $0.85 \cdot h_{gap}$, a rapid reduction in C_p is observed near the top edge of the face, which highlights the influence of the MSBC system in comparison to the effect of cab fairing. This reduction in C_p is caused by the suction of the flow from the front of the face resulting in a significant reduction in the extent of high pressure region. As can be seen from Fig. 13(a), the moving surface causes a downward shift in the high pressure region location.

Figure 13(b) shows the pressure distribution on the rear face of the semi-trailer for the configuration with the MSBC system. Low pressure regions with C_p less than -0.5 are observed up to a height of $0.15 \cdot h_{trailer}$. This is much lower compared to the baseline configuration (Fig. 8(b)) as well as that with the cab fairing. Further it is seen that the pressure distribution is substantially similar to the baseline configuration and that with the cab fairing for the middle region that extends from a height of $0.25 \cdot h_{trailer}$ to $0.65 \cdot h_{trailer}$. The asymmetric low pressure region found in the baseline configuration and that with the cab fairing towards the left side of the face is observed to be substantially reduced. This can be further seen by the significantly more uniform distribution of pressure for $y > 0.65 \cdot h_{trailer}$.

Fig. 13(a) Pressure distribution on the front face of semi-trailer with the MSBC system only.
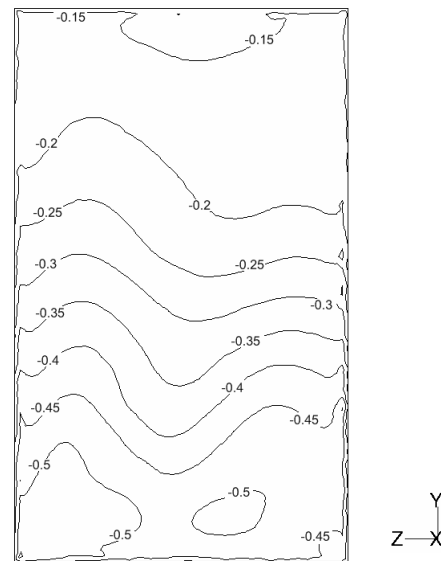

Fig. 13(b) Pressure distribution on the rear face of semi-trailer with the MSBC system only.
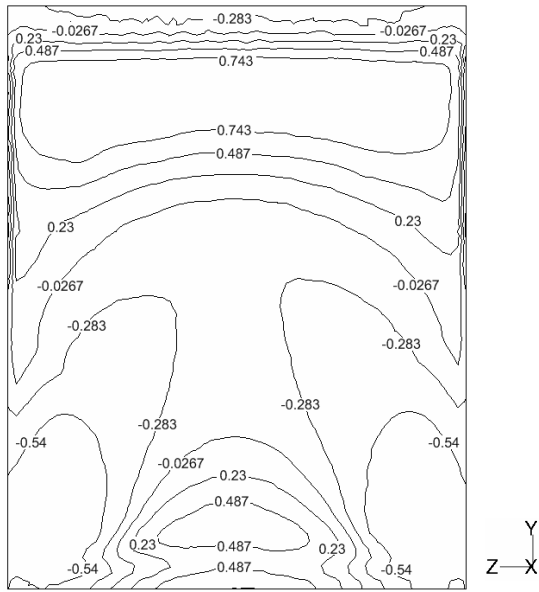
Fig. 14(a) Pressure distribution on the front face of semi-trailer with the cab fairing and MSBC system.
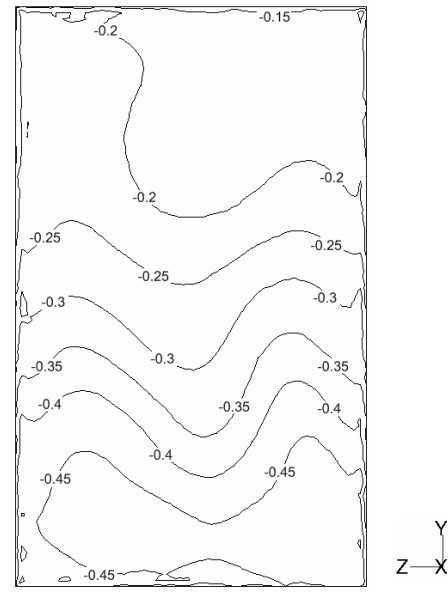

Fig. 14(b) Pressure distribution on the rear face of semi-trailer with the cab fairing and MSBC system.

Figure 14(a) shows the pressure distribution on the front face of the semi-trailer when the base line semi-trailer is equipped with both the cab fairing and the MSBC. The lower part of the face exhibits a pressure distribution qualitatively similar to the configuration with the cab fairing with a small region of high pressure ($C_p > 0.485$) near the bottom. Small regions of lower pressure ($C_p > -0.54$) are also observed near the sides of the face in this region, each of which extends $0.27 \cdot h_{gap}$ in height and $0.2 \cdot w_{trailer}$ in width. The middle region of the semi-trailer front face ($0.27 \cdot h_{gap} < y < 0.66 \cdot h_{gap}$) exhibits predominantly low pressure with C_p between -0.0267 and -0.283. The pressure rises to $C_p > 0.743$ near the top region of the face for ($0.8 \cdot h_{gap} < y < 0.9 \cdot h_{gap}$). At the top the influence of the MSBC system is clearly visible as the pressure along the height of the face above height of $0.9 \cdot h_{gap}$ sharply decreases. It is clear from the above discussion that the reduction in the high pressure region on the front face of semi-trailer has two components, first the cab fairing which pushes the high pressure region up and second, the MSBC which moves the high pressure region in the downward direction. The cab roof fairing shields a larger area of the front face of trailer from the oncoming flow and the moving surface of the MSBC system provides suction. This shows that the influence of the MSBC system is specific to the upper region of the face which contains the peak pressure.

Figure 14(b) shows the pressure distribution on the rear face of the semi-trailer for the configuration with the both the cab fairing and

MSBC system. Low pressure regions with C_p less than -0.45 are observed up to a height of $0.15 \cdot h_{trailer}$. This region is larger compared to the configuration with the cab fairing (Fig. 12(b)). Further it is seen that for the middle region that extends from a height of $0.25 \cdot h_{trailer}$ to $0.65 \cdot h_{trailer}$ pressure distribution is substantially similar to all the three configurations of the tractor-trailer combination discussed earlier (Fig. 8(b), Fig. 12(b) and Fig. 13(b)). Similar to the front face of the semi-trailer discussed earlier (Fig. 12(a) and Fig. 13(a)) it is seen that the influence of the two add-on devices on the pressure distribution on the rear face of the semi-trailer is also cumulative. Non-uniformity in variation of pressure was observed for all the four configurations at heights of $0.1 \cdot h_{trailer}$ and $0.9 \cdot h_{trailer}$. These variations may be associated with the presence of flow structures, mainly contra rotating vortices in the wake of the semi-trailer, which are also seen later in velocity vector plots.

The distribution of pressure on both front and rear faces of the semi-trailer with and without add-on devices is quite complex. The pressure field is symmetrical about the longitudinal symmetry plane over a large face area. For the tractor-trailer configuration with the cab roof fairing, the MSBC system and the configuration equipped with a combination of both of these add-on devices, the spatial extent of this high pressure region is reduced. Thus, the overall pressure on the semi-trailer front face is substantially reduced.
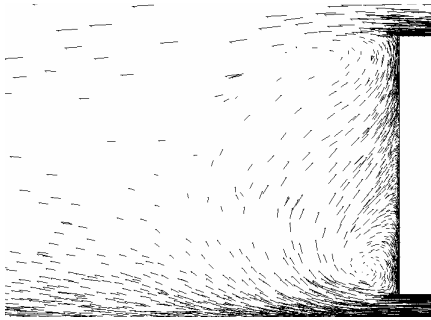
Fig. 15(a) Velocity vectors along the X-Y symmetry plane for cab fairing only – wake.
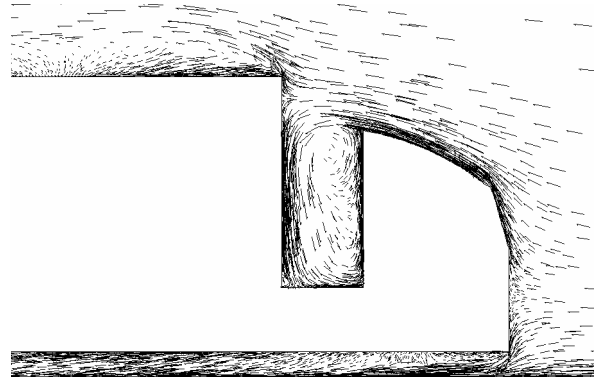

Fig. 15(b) Velocity vectors along the X-Y symmetry plane for cab fairing only – tractor-trailer gap.
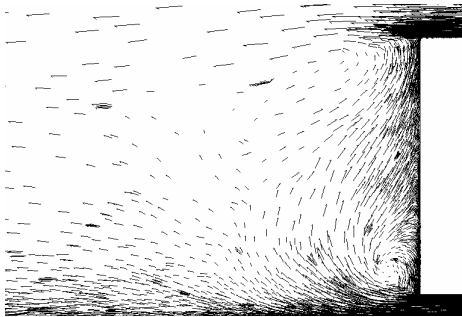

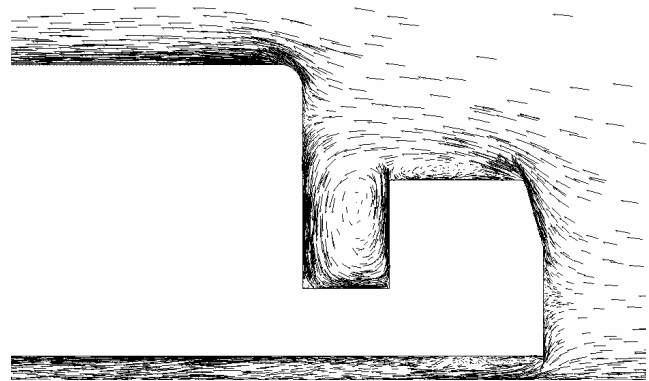Fig. 15(c) Velocity vectors along the X-Y symmetry plane for MSBC only – wake.

Fig. 15(d) Velocity vectors along the X-Y symmetry plane for MSBC only – tractor-trailer gap.
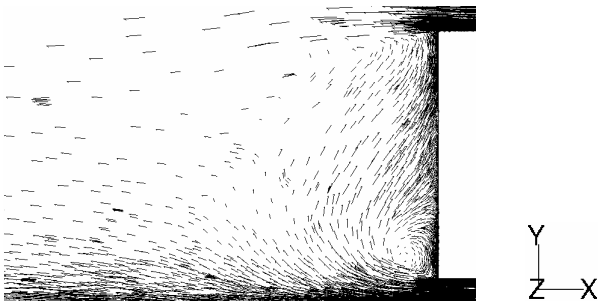

Fig. 15(e) Velocity vectors along the X-Y symmetry plane for cab fairing and MSBC – wake.
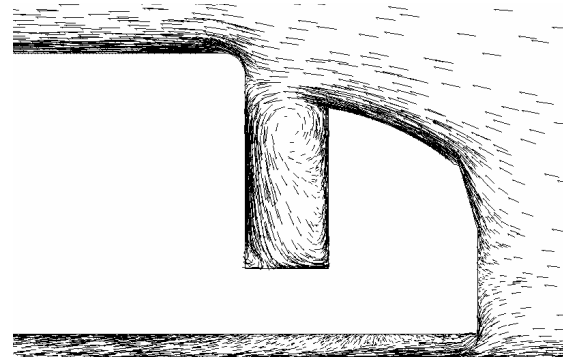
Fig. 15(f) Velocity vectors along the X-Y symmetry plane for cab fairing and MSBC – tractor-trailer gap.

Velocity vectors plotted on the vertical longitudinal symmetry plane are shown in Fig. 15. Figure 15(a), (c) and (e) show the presence of a recirculation region immediately downstream of the semi-trailer. This region consists of two contra rotating vortices also observed in the wake of the baseline tractor-trailer. The lower clockwise vortex is observed to be much larger than the upper counter-clockwise vortex. This was also observed in the wake of the baseline configuration discussed earlier. Fig. 15(e) shows that the upper counter-clockwise vortex for the tractor-trailer combination equipped with the cab fairing and the MSBC system is significantly smaller as compared to that for other configurations investigated.

Figure 15(b) shows the flow pattern in the tractor-trailer gap for the tractor-trailer configuration

equipped with the cab fairing. In this configuration the flow can be seen to impact on the semi-trailer front face at a higher point than that for the baseline configuration. This corresponds to the upward shift in the high pressure region as discussed earlier (see Fig. 12(a)). The cab fairing eliminates the formation of the recirculation bubble above the cab roof, which was seen in the baseline configuration (see Fig. 12(a)). However the cab fairing fails to influence flow separation at the leading edge of the semi-trailer. In comparison, Fig. 15(d) shows the flow pattern in the tractor-trailer gap for the configuration with the MSBC system only. The moving surface of the MSBC system injects sufficient kinetic energy into the flow to completely eliminate flow separation on the semi-trailer roof. In addition, the MSBC system provides a suction of flow from the front of the rotating cylinder in the gap. This corresponds to the downward shift in the high pressure regions discussed earlier (see Fig. 13(a)). In Fig. 15(f), it can be seen that the flow is fully attached on the roof of the semi-trailer (in case of the configuration with a combination of cab fairing and the MSBC system). The flow patterns in the tractor-trailer gap indicate that the cab fairing deflects the oncoming air stream to impact semi-trailer front face at a higher point. The MSBC system reduces the high pressure on the front face of the semi-trailer because of suction of flow from the tractor-trailer gap. Both these devices complement each other in reducing the spatial extent of the high pressure region. This was also seen earlier in the distribution of C_p on the semi-trailer front face (see Fig. 14(a)).
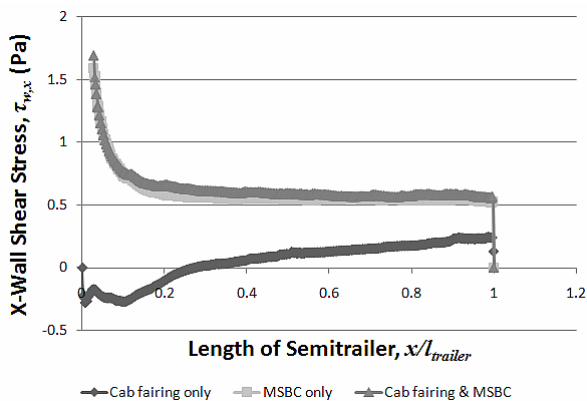
longitudinal centre line on the semi-trailer top surface. A plot of streamwise shear stress on the top surface of the semi-trailer is shown in Fig. 16. In both configurations of the tractor-trailer where MSBC is employed, it is observed that shear stress values are extremely high near the leading edge of the semi-trailer ($x/l_{trailer} < 0.2$). This can be attributed to the moving surface that provides the additional kinetic energy to the flow near the surface. Further, it is also seen that shear stress remains positive for the entire length of the semi-trailer. This indicates that streamwise velocity near the surface is positive (i.e., in the direction of free stream flow) and represents fully attached flow. Further optimisation of the MSBC system may be carried out by studying the influence of rotational velocity of the cylinder on the shear stress. Shear stress profile for configuration with the cab fairing shows qualitative similarity to that of the baseline configuration (described in Fig. 10). Shear stress for the configuration with only the cab fairing shows a change in direction at $x/l_{trailer} = 0.272$. This is the point where the shear stress becomes positive and acts in the direction of the free stream flow. It is representative of positive streamwise velocity near the surface. This indicates that the flow reattaches to the top surface of the semi-trailer at a distance of $x/l_{trailer} = 0.272$.
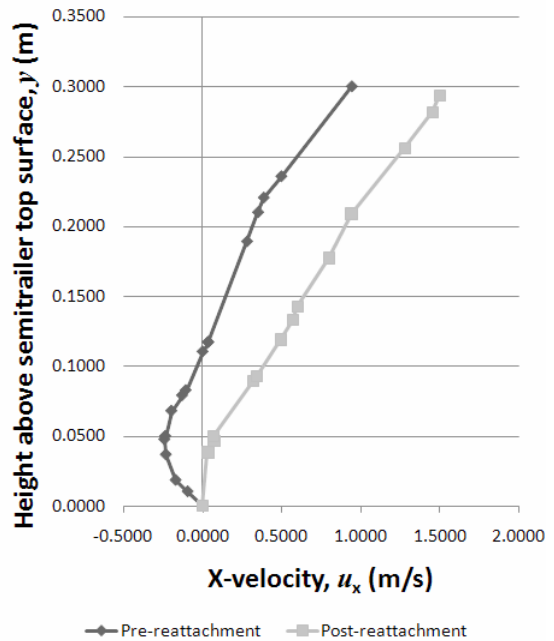
Fig. 16   Streamwise wall shear stress profile on the top surface of the semi-trailer.

Fig. 17   Streamwise (X) velocity profile in boundary layer of semi-trailer roof.

Separation of flow at the leading edge of the semi-trailer for the configurations with various combinations of add-on devices can be further studied by wall shear stress variation along the

This point of flow reattachment is validated by mapping the velocity profile in the boundary layer before and after the reattachment point at $x/l_{trailer}$

values of 0.271 and 0.276 respectively. These profiles are shown in Fig. 17, which shows a negative value for streamwise velocity up to a height of 0.11 m above the semi-trailer roof.

5.4 Pressure field in tractor-trailer gap

The flow field in the tractor trailer gap affects the drag force acting on the vehicle considerably (Allan, 1981). The flow field in the gap depends considerably on the difference in the height of the tractor cab and the double-deck semi-trailer.

Figure 18 shows the variation of pressure coefficients averaged over five planes placed at equidistant locations within the gap such that the distance between two planes 25% of the gap length starting from the rear face of the tractor up to the front face of the semi-trailer. It is seen from this profile that all configurations of the tractor-trailer combination show significant qualitative similarity in pressure distribution. Pressure at the back of the tractor cab is observed to be low with negative values of C_p. For the configurations with the cab fairing, a much lower average pressure of $C_p \approx -0.3$ is observed. For the two configurations without the cab fairing average pressures are observed to be relatively higher at $C_p \approx -0.1$. As the distance x, in the gap along the streamwise direction increases (non-dimensionalised relative to the length of the gap, l_{gap}), average C_p increases for all the configurations investigated. However this peak value is highest for the baseline configuration with $C_p = 0.43$. The average pressure for the configuration with the MSBC system is next lower with $C_p = 0.24$, followed by the configuration with the cab fairing with $C_p = 0.15$ and finally the configuration with the combination of cab fairing and the MSBC system having a lowest average pressure on the semi-

trailer front face with $C_p = 0.09$. The comparison of average pressure variation in the tractor-trailer gap clearly indicates that both configurations with the MSBC system show a reduced pressure rise within the gap.

5.5 Differential pressure across semi-trailer length

Presence of flow structures in the flow-field of the tractor-trailer combination influences the distribution of pressure on the surface of the vehicle. The earlier discussion described this distribution of pressure on the front and rear faces of the semi-trailer. The difference in pressure between the front and rear faces of the semi-trailer can be computed to quantify the pressure drag.

The average C_p on the front and rear faces of the semi-trailer for all the four configurations of the tractor-trailer was computed and is shown in Table 3. Both the cab fairing as well as the MSBC system have been found to be effective in reducing the average C_p on the front face of the semi-trailer.

The average C_p on the front face of the semi-trailer was found to be 0.43, 0.15, 0.24 and 0.09 for the baseline configuration and those with the cab fairing, the MSBC system and a combination of both devices respectively. Similarly, the average C_p on the rear face of the semi-trailer was found to be respectively -0.28, -0.27, -0.29 and -0.28 for the configurations described above. The resulting difference in pressure coefficient (ΔC_p) between these two faces of the semi-trailer was calculated and is also shown in Table 3. The differential pressure coefficient ΔC_p was found to be 0.71, 0.42, 0.53 and 0.37 respectively for the four tractor-trailer configurations mentioned
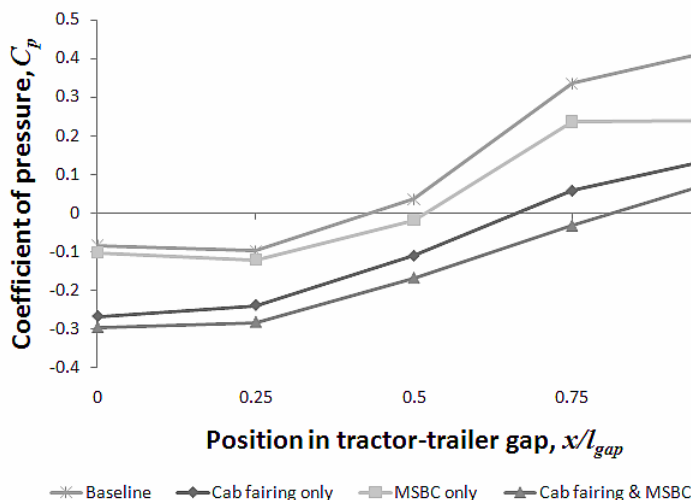

Fig. 18   Average pressure profile in tractor-trailer gap.

Table 3 Pressure difference between front and rear faces of the semi-trailer for various configurations of the tractor-trailer combination.

Tractor-trailer Combination	Average Coefficient of Pressure C_p		Average Differential Pressure Coefficient ΔC_p
	Semi-trailer front face	Semi-trailer rear face	
Baseline	0.4290	-0.2763	0.7053
Cab fairing only	0.1478	-0.2659	0.4137
MSBC only	0.2404	-0.2904	0.5307
Cab fairing and MSBC	0.0914	-0.2810	0.3724

above. The value of ΔC_p for the configuration with the MSBC system is higher than that with the cab fairing by 0.11. However it will be seen in the following discussion that the MSBC system compensates for this by having a larger influence tractor cab drag. When used in combination, the cab fairing and the MSBC system result in a substantially lower overall ΔC_p for the semi-trailer. This results in significantly lower overall pressure drag acting on the vehicle.

5.6 Coefficient of drag

Table 4 shows a comparison of overall drag coefficient (C_D) of the three combinations of aerodynamic devices with the baseline configuration. The C_D for the baseline configuration without any aerodynamic device was found to be 0.9. With the addition of the MSBC system to the baseline configuration the C_D was reduced to 0.78, a 13% reduction. This reduction is comparable to that achieved when the

Table 4 Comparison of overall drag coefficient.

Configuration	Coefficient of drag, C_D
Baseline	0.90
Cab fairing only	0.78
MSBC only	0.79
Cab fairing and MSBC	0.70

cab fairing was used with baseline configuration. It can further be seen that when used in combination with the cab fairing the MSBC system provides a further reduction in C_D by 9% to 0.7 – an overall reduction of 22% in drag.

Individual contributions of the tractor cab, the semi-trailer and the wheels of the tractor-trailer combination to the overall drag are shown in Table 5. A comparison of these contributions shows that using the cab fairing reduces the C_D of the semi-trailer from 0.57 to 0.38. This is achieved by shielding the front face of the semi-trailer from the oncoming flow. When the MSBC system is used alone the C_D of both the tractor cab as well as the semi-trailer is reduced from 0.26 to 0.2 and from 0.57 to 0.46 respectively.

Further, it is seen that when a combination of both these devices is used the C_D of the semi-trailer is reduced from 0.57 to 0.29. The above discussion has clearly indicated the effectiveness of MSBC system in reducing the drag.

5.7 Motive power reduction

Based on the drag coefficients obtained earlier the aerodynamic drag force at various vehicle velocities has been computed and is shown in Fig. 19. It is seen that the drag force increases with the vehicle speed. At low vehicle speeds (10 mile/hour, 4.5 m/s) the reduction in drag force

Table 5 Individual drag coefficient of each section of the semi-trailer combination for various configurations investigated.

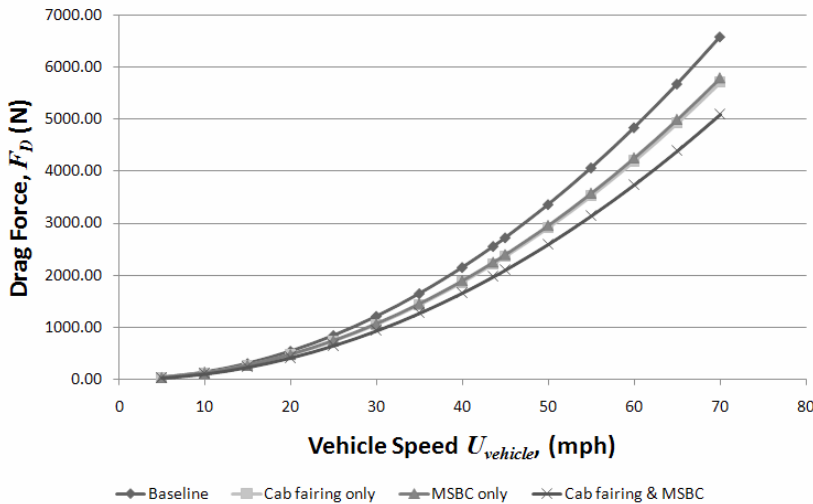| Tractor-trailer Combination	Tractor cab		Semi-trailer		Wheels	
	Coefficient of drag C_D	Percentage contribution to overall drag	Coefficient of drag C_D	Percentage contribution to overall drag	Coefficient of drag C_D	Percentage contribution to overall drag
Baseline	0.2593	28.82%	0.5696	63.29%	0.0704	7.82%
Cab fairing only	0.2599	33.36%	0.3792	48.68%	0.0717	9.21%
MSBC only	0.1961	24.80%	0.4625	58.49%	0.0721	9.12%
Cab fairing and MSBC	0.2617	37.58%	0.2928	42.05%	0.0751	10.78%

Fig. 19   Overall drag force acting on tractor-trailer combination at various speeds.
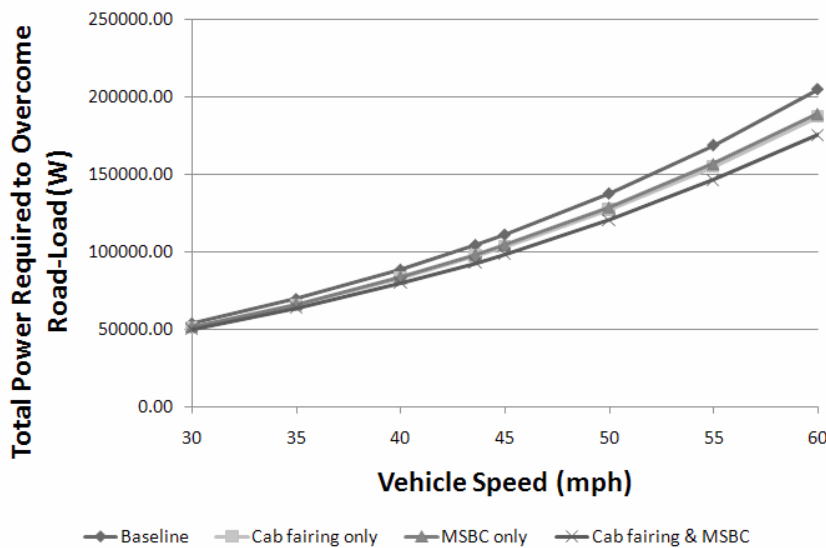

Fig. 20   Motive power requirement at various speeds.

by using both the cab fairing and the MSBC system, although higher than other configurations, is only 30 N. However at higher cruising speed of 25 m/s (55 mile/hour, 89 km/hour) aerodynamic drag becomes the most dominant resistance force encountered by the moving vehicle. This reduction in drag force rises to 923 N. The combination of the cab fairing and the MSBC system at this speed provides reduction in aerodynamic drag of up to 22%.

Figure 20 shows the power required by a typical tractor trailer, with various combinations as discussed above, at different cruise velocities between 30 and 60 mile/hour. A rolling resistance of 2795.85N is considered on the basis of a generic laden tractor-trailer weighing 38000 kg (RoadTransport.com, 2007). The figure shows that the motive power required in overcoming various resistances increases with the steady-state vehicle speed. It has been found that using a combination of the cab fairing and the MSBC

system resulted in around 13% (23 kW) reduction in power consumption at motorway speeds of 55 mile/hour (25 m/s, 89 km/hour) as compared to the baseline tractor-trailer combination. The motive power required to rotate the rotating cylinder MSBC device can be provided by a standard DC motor integrated into the retrofit assembly. An estimate of the power drawn by the motor can be made by considering an aluminium cylinder weighing between 20 and 50 kg. The power required by the motor will be approximately 1.8 kW (Munshi, Modi & Yokomizo, 1999).

5.8   Fuel savings

At about 25 m/s (55 mile/hour, 89 km/hour) aerodynamic drag is the most dominant resistance force and the MSBC system provides a reduction in power consumption of 7% from 169 kW to 157 kW; when combined with the cab fairing it provides a further 6% reduction in power

consumption down to 146 kW. At this speed, energy saved per mile travelled (E) based on 23 kW reduction in power consumption is given by the following equation:

$$E = \frac{P}{V} = \frac{23 \times 10^3 \; W}{55 \; mile / hour} = 418.18 \; W \cdot hour / mile \qquad (6)$$

The energy density of diesel (ξ_{diesel}) is 10.9×10^3 W·h/litre (Transtronics Inc., 2008); thus the improvement in fuel efficiency (φ) can be computed by using the following equation:

$$\varphi = \frac{E}{\xi} = \frac{418.18 \; W \cdot hour / mile}{10.9 \times 10^3 \; W \cdot hour / litre} = 0.038 \; litre / mile \qquad (7)$$

Thus, a 13% reduction in power consumption provides a reduction in fuel consumption of 0.0384 litre/mile, which is more than 6% of the average HCV fuel consumption of 0.5747 litre/mile (2.8 km/litre) (Department for Transport, 2006). This clearly shows the huge potential of the MSBC system to reduce overall fuel consumption without making any major alterations to the shape or overall dimensions of the vehicle. Such a significant reduction in overall fuel consumption by even a small fleet of vehicles will result in a similar reduction in emissions, thus making commercial vehicles more environment-friendly.

6. CONCLUSIONS

Flow field analysis of a simplified model of a generic tractor-trailer combination was carried out at nominal cruising velocity. Velocity and pressure distribution in the flow field were evaluated and compared. It was observed that the injection of momentum reduces the individual drag acting on both the tractor cab and the semi-trailer. Closer observation of flow separation and reattachment points indicated that addition of the cab roof fairing induces earlier reattachment of the flow, thus reducing the size of the recirculation bubble on the roof of the semi-trailer. The MSBC on the other hand completely prevents separation of flow at the leading edge of the semi-trailer. It can be concluded from the discussions above that the reduction in drag achieved by the combination of the MSBC system and the cab fairing is a result of cumulative effect of the influence of both devices on the flow field around the tractor-trailer combination.

The reduction in aerodynamic drag achieved by the MSBC device when used alone is comparable to that achieved by the cab roof fairing alone. Furthermore, this device makes the aerodynamic

efficiency of the semi-trailer independent of the tractor unit it is coupled with, thus providing operational flexibility to freight operators. The proposed device, when used in combination with the cab fairing provides a 13% (23 kW) reduction in power consumption as compared to a baseline double deck tractor-trailer. The maximum power required to drive the rotating cylinder is 1.8 kW which is only 8% of the overall power savings achieved. The reduction in power consumption achieved by this device will result in reduction in fuel consumption of approximately 2.1 million litres per annum for a typical large fleet of tractor-trailers. At 92 pence/litre (Cole, 2008), this will save about £1.9 million per annum.

NOTATIONS

C_D	coefficient of drag
E	energy per mile distance traveled (W·h/mile)
F	external force (N)
F_D	aerodynamic drag force (N)
g	acceleration due to gravity (m/s^2)
h	overall height of tractor-trailer combination (m)
h_{gap}	height of the tractor-trailer gap, from bottom of semi-trailer front face to its top (m)
$h_{trailer}$	height of the semi-trailer, from bottom of the vehicle to top of semi-trailer (m)
I	unit tensor
k	turbulent kinetic energy (m^2/s^2)
l	overall length of the tractor-trailer combination (m)
l_{cab}	length of cab (m)
l_{gap}	length of tractor-trailer gap, from back of tractor cab to front of semi-trailer (m)
$l_{trailer}$	length of semi-trailer (m)
m	mass (Kg)
p	static pressure (Pa)
P	power (W)
Re	Reynolds number
S_m	mass source
t	time (s)
v, V	velocity (m/s)
w	overall width of the tractor-trailer combination (m)
x	streamwise (longitudinal) position (m)
y	vertical position (m)
z	lateral position (m)

Greek

∇ gradient operator

ε turbulence dissipation rate (m^2/s^3)

λ ratio of cylinder surface velocity to free-stream velocity

μ dynamic viscosity (molecular) $(N{\cdot}s/m^2)$

ξ energy density of fuel (diesel) $(W{\cdot}h/mile)$

ρ density (Kg/m^3)

τ shear stress (Pa)

φ fuel consumption (l/mile)

ω specific dissipation rate (s^{-1})

Ω angular velocity (rad/s)

Subscripts

angular   angular (velocity)

air   of air

cylinder   of the rotating cylinder

D   of drag

diesel   of diesel

gap   of the tractor-trailer gap

trailer   of the trailer

Abbreviations

CFD   Computational Fluid Dynamics

HCV   Heavy Commercial Vehicle

MSBC   Moving Surface Boundary-layer Control (momentum injection)

SST   Shear-Stress Transport

REFERENCES

1. Allan J (1981). Aerodynamic drag and pressure measurements on a simplified tractor-trailer model. *Journal of Wind Engineering and Industrial Aerodynamics* 9(1–2):125–136.

2. Cole L (2008). *Diesel Prices and Fuel Tax*. RoadTransport.com. Available at: http://www.roadtransport.com/Articles/2008/02/27/130000/diesel-prices-and-fuel-tax.html (Accessed September 12, 2008).

3. Department for Transport (2006). *Smoothing the Flow at TNT Express and Somerfield Using Truck Aerodynamic Styling*. Freight Best Practice. Available at: http://www.freightbestpractice.org.uk/default.aspx?appid=1960&cid=42 (Accessed July 29, 2008).

4. DON-BUR, Aerodynamic Teardrop Trailer. DON-BUR. Available at: http://www.donbur.co.uk/gb/products/aerodynamic_teardrop_trailer.shtml (Accessed September 11, 2008).

5. Englar R (2000). *Development of Pneumatic Aerodynamic Devices to Improve the Performance, Economics, and Safety of Heavy Vehicles (2000-01-2208)*, Washington, DC (USA): Society of Automotive Engineers (SAE). Available at: http://www.osti.gov/bridge/servlets/purl/770965-K88tPq/native/770965.pdf (Accessed September 19, 2008).

6. Fluent Inc. (2006). *FLUENT 6.3 User's Guide*.

7. Fluent Inc. (2007). *GAMBIT 2.4 User's Guide*.

8. Hucho WH, ed. (1998). *Aerodynamics of Road Vehicles*. 4th ed., Warrendale, PA (USA): Society of Automotive Engineers (SAE).

9. Malviya V, Mishra R, Fieldhouse J (2008). Comparative computational analysis of drag-reducing devices for tractor-trailers. In G Lucas & Z Xu, eds. *Proceedings of Computing and Engineering Annual Researchers' Conference 2008*. Huddersfield (UK): University of Huddersfield, pp. 1–8. Available at: http://eprints.hud.ac.uk/3669/1/3.pdf (Accessed January 30, 2009).

10. Matěj S, Jiří N (2004). Aerodynamic devices to reduce the base- and underbody drag of semitrailer unit. In *AED2004: sborník příspěvků 4th International Conference on Advanced Engineering Design na CD*. Glasgow (UK): Orgit Ltd. Available at: http://www3.fs.cvut.cz/web/fileadmin/documents/12241-BOZEK/publikace/2004/AED2004_Sulitka.pdf (Accessed August 5, 2008).

11. Menter F (1994). Two-equation eddy-viscosity turbulence models for engineering applications. *AIAA Journal* 32(8):1598–605.

12. Modi V (1991). Moving surface boundary-layer control – studies with bluff-bodies and application. *AIAA Journal* 29(9):1400–1406.

13. Modi V (1997). Moving surface boundary-layer control: A review. *Journal of Fluids and Structures* 11(6):627–663.

14. Modi V, Fernando M, Yokomizo T (1991). Moving surface boundary-layer control as applied to two-dimensional and three-dimensional bluff bodies. *Journal of Wind Engineering and Industrial Aerodynamics* 38(1):83–92.

15. Modi V, Ying B, Yokomizo T (1992). Effect of momentum injection on the aerodynamics of several bluff bodies. *Journal of Wind Engineering and Industrial Aerodynamics* 41(1–3):713–714.

16. Munshi S, Modi V, Yokomizo T (1999). Fluid dynamics of flat plates and rectangular prisms in the presence of moving surface boundary-layer control. *Journal of Wind Engineering and Industrial Aerodynamic*s 79(1–2):37–60.

17. Régert T, Lajos T (2007). Description of flow field in the wheelhouses of cars. *International Journal of Heat and Fluid Flow* 28(4):616–629.

18. RoadTransport.com (2007). Weights and Dimensions/Vehicle Plating. RoadTransport.com. Available at: http: / / www. roadtransport. com / RoadLegal / 11947 / weights - dimensions - plating. html (Accessed July 22, 2008).

19. Roberts P (2008). World Oil. *National Geographic Magazine*. Available at: http://ngm.nationalgeographic.com/print/2008 /06/world-oil/roberts-text (Accessed January 4, 2009).

20. Rose MJ (1981). Commercial vehicle fuel economy – The correlation between aerodynamic drag and fuel consumption of a typical truck. *Journal of Wind Engineering and Industrial Aerodynamics* 9(1–2):89–100.

21. Shih T et al. (1995). A new k-ε eddy viscosity model for high Reynolds number turbulent flows. *Computers & Fluids* 24(3):227–238.

22. Singh S et al. (2005). Effect of moving surface on the aerodynamic drag of road vehicles. *Proceedings of the Institution of Mechanical Engineers, Part D: Journal of Automobile Engineering* 219(2):127–134.

23. Transtronics Inc. (2008). Energy density. *Transtronics Home of Automation*. Available at: http://wiki.xtronics.com/index.php/Energy _density (Accessed September 12, 2008).

24. Versteeg H, Malalasekera W (1995). *An Introduction to Computational Fluid Dynamics: The Finite Volume Method*, Prentice Hall.

25. Wood R, Bauer S (2003). Simple and low-cost aerodynamic drag reduction devices for tractor-trailer trucks (2003-01-3377). In *International Truck & Bus Meeting & Exhibition*. Ft. Worth (TX), USA: Society of Automotive Engineers (SAE), p. 18. Available at: http : / / www.solusinc.com / pdf / 2003 - 01 - 3377.pdf (Accessed January 27, 2009).